

Daytime Isoprene Nitrates Under Changing NO_x and O₃

Alfred W. Mayhew¹, Peter M. Edwards¹, Jaqueline F. Hamilton^{1,2}

¹ Wolfson Atmospheric Chemistry Laboratories, Department of Chemistry, University of York, Heslington, York, UK

² National Centre for Atmospheric Science, University of York, York, UK

5 *Correspondence to:* Jaqueline F. Hamilton (jacqui.hamilton@york.ac.uk)

Abstract. Organonitrates are important species in the atmosphere due to their impacts on NO_x, HO_x, and O₃ budgets, and their potential to contribute to secondary organic aerosol (SOA) mass. This work presents a steady-state modelling approach to assess the impacts of changes in NO_x and O₃ concentrations on the organonitrates produced from isoprene oxidation. The diverse formation pathways to isoprene organonitrates dictate the responses of different groups of organonitrates to changes in O₃ and NO_x. For example, organonitrates predominantly formed from the OH-initiated oxidation of isoprene favour formation under lower ozone and moderate NO_x concentrations, whereas organonitrates formed via day-time NO₃ oxidation show the highest formation under high O₃ concentrations with little dependence on NO_x concentrations. Investigating the response of total organonitrates reveals complex and non-linear behaviour with implications that could inform expectations of changes to organonitrate concentrations as efforts are made to reduce NO_x and O₃ concentrations, including a region of NO_x-O₃ space where total organonitrate concentration is relatively insensitive to changes in NO_x and O₃. These conclusions are further contextualised by estimating the volatility of the isoprene organonitrates revealing the potential for high concentrations of low volatility species under high ozone conditions.

1 Introduction

Organonitrates are important species in the atmosphere due to their potential to impact on NO_x, HO_x, and O₃ budgets through gas-phase chemistry.(Emmerson and Evans, 2009; Bates and Jacob, 2019; Schwantes et al., 2019; Schwantes et al., 2020; Vasquez et al., 2020) Their relatively low volatility also results in the potential to form secondary organic aerosol (SOA) via condensation onto existing particles, and some organonitrates can undergo reactive uptake to the particle phase.(Hallquist et al., 2009; Schwantes et al., 2019; Palmer et al., 2022) Isoprene organonitrates have been widely studied due to the large emissions of isoprene resulting in the relevance of isoprene chemistry to a range of environments around the globe. (Guenther et al., 2006; Pye et al., 2015; Reeves et al., 2021; Tsiligiannis et al., 2022)

Isoprene hydroxynitrate (IHN) is widely studied due to its formation from OH oxidation in the presence of NO resulting in high concentrations during the daytime (Figure 1).(Xiong et al., 2015; Wennberg et al., 2018) IHN also has formation routes from oxidation with the nitrate radical (NO₃). Other commonly studied isoprene mononitrates include isoprene carbonyl nitrate (ICN) and isoprene hydroperoxy nitrate (IPN). IPN forms through the initial NO₃ oxidation of isoprene to form an isoprene nitrooxyperoxy radical (INO₂). Reaction of INO₂ with HO₂ then forms IPN. ICN has a range of formation pathways initiated by OH and NO₃ oxidation. Isoprene dinitrate (IDN) can also form from INO₂ by its reaction with NO.

Isoprene epoxides, such as isoprene epoxydiols (IEPOX), have long been of interest due to their potential to contribute to SOA by reactive uptake to acidified particles. (Paulot et al., 2009; Surratt et al., 2010) Later work outlined the similar SOA-forming properties for the nitrated epoxide, isoprene nitrooxyhydroxy epoxide (INHE), with the first proposed formation route to INHE involving the OH oxidation of IPN (Figure 2).(Schwantes et al., 2015) Recent work aiming to improve the representation of isoprene NO₃ chemistry in chemical mechanisms highlighted a previously unrepresented reaction pathway to forming nitrated epoxides from alkoxy radicals (RO). (Vereecken et al., 2021; Carlsson et al., 2023) This alkoxy-epoxidation pathway provides an alternative formation route to INHE that doesn't rely on a stable intermediate or the presence of OH (Figure 3). Additionally, three more nitrated epoxides can result from this pathway: isoprene nitrooxycarbonyl epoxide (INCE), isoprene nitrooxyhydroperoxy epoxide (INPE), and isoprene dinitrooxy epoxide (IDNE). The motivation for the work presented here stems from findings from the 2017 Atmospheric Pollution and Human Health in a Chinese Megacity (APHH) summer campaign in Beijing, showing the role of NO₃ in the formation of isoprene organonitrates and their successive particle-phase products, including in the afternoon due to the presence of high O₃ concentrations. (Hamilton et al., 2021; Newland et al., 2021) The presence of high O₃ concentrations increased the conversion of NO to NO₂ which subsequently reduced the loss of NO₃ to reaction with NO. Geyer *et al.* first highlighted this in 2003, calculating daytime NO₃ mixing ratios of up to 2-5ppt during the afternoon during a haze period in La Porte, Texas.(Geyer, 2003) Since then, daytime NO₃ has been highlighted as a potentially important chemical pathway from a range of field campaigns in various cities around the world. (Brown et al., 2005; Osthoff et al., 2006; Khan et al., 2015; Xue et al., 2016; Wang et al., 2020; Foulds et al., 2021) Daytime NO₃ chemistry has also been shown to be potentially significant under forest canopies, where photolytic processes are diminished. (Forkel et al., 2006; Hu et al., 2013; Mermet et al., 2021) The co-occurrence of organonitrate formation from OH and NO₃ chemistry, along with the multi-stage chemistry often required for their formation, results in the potential for complex dependencies on NO_x and O₃ concentrations. However, these NO_x and O₃ dependencies have not previously been investigated. This work describes efforts to investigate the sensitivity of daytime isoprene organonitrate chemistry to changes in NO_x and O₃ concentrations through a series of steady-state models. This work also aims to identify the role of O₃ concentrations in daytime NO₃ chemistry and determine the NO_x and O₃ concentrations that facilitate this understudied reaction pathway. While the data presented here solely focusses on nitrated species resulting from isoprene, similar variations in organonitrate speciation under different NO_x-O₃ regimes are likely to hold for any VOC which can undergo oxidation by both OH and NO₃ radicals.

2 Experimental

2.1 Model Description

The goal of this work is to investigate changes in NO_x and O₃ on the chemistry of isoprene nitrates in the afternoon period in Beijing. To do this, the models should demonstrate the favoured reaction pathways under different oxidant concentrations in the absence of other variables. This means that physical and photolytic processes should be held constant, i.e. the models will describe the chemistry occurring at a representative point in the day. Species must also be allowed to reach their steady-state concentrations in order to eliminate the role of the model spin-up period on resultant species concentrations.

Comparison of the concentrations of species in these so-called steady-state models then allows for conclusions to be drawn as to the preferred oxidation products under various conditions.

All models described in this work were run using AtChem2, an open-source zero-dimensional box model. (Sommariva et al., 2019) All models also made use of the Isoprene mechanism published by Vereecken *et al.* 2021 (henceforth the FZJ Mechanism) which aimed to improve the representation of NO₃ chemistry of isoprene by building on chemistry from the Master Chemical Mechanism (MCM) and the review of isoprene chemistry published by Wennberg *et al.* (Jenkin et al., 2015; Wennberg et al., 2018; Vereecken et al., 2021; Carlsson et al., 2023) In order to make the species naming consistent between the MCM portion and the added chemistry of the FZJ mechanism, ISOPCNO₃ was renamed to EISOP1N4OH as both identical species are present in the original FZJ mechanism.

The steady-state models are sets of models run at a range of fixed NO_x and O₃ mixing ratios. Models were run for NO_x mixing ratios up to 45 ppb and O₃ mixing ratios of 140 ppb, corresponding to the upper limit of measurements made in the Beijing 2017 campaign. (Shi et al., 2019) In order to provide additional OH reactivity, a constant concentration of methane was added to all of the models to ensure that the modelled OH reactivity matched measured values under Beijing-like conditions, this is discussed further in the Model Validation section. The required mixing ratio corresponded to 82 ppm of methane in all of the models. The modelled concentration of species is taken as the final concentration after 5 model days, after all species had been allowed to reach steady-state concentrations. Each model was run at photolysis conditions corresponding to those calculated by AtChem2 for 16:00 local time in Beijing, China. This was around the time of peak daytime NO₃ concentrations in Beijing, before concentrations rapidly increased during sunset. To ensure steady-state was reached in a reasonable time, and to provide loss routes for species without losses, species were removed from the model at a dilution rate of $2.31 \times 10^{-5} \text{ s}^{-1}$, corresponding to a dilution lifetime of 12 hours. This value was selected based on a combination of the physical loss processes included in previous modelling work, and the impact of this decision is assessed in Section 3.1. (Mayhew et al., 2022; Edwards et al., 2014; Edwards et al., 2013)

All models were run at a temperature of 298.15 K, a pressure of 1013 mbar, and a relative humidity of 50%. The latitude, longitude, and date used for photolysis calculations were 39.909°, 116.398°, and 2022-06-01. NO_x was constrained by adjusting the NO and NO₂ concentrations at the beginning of each time step such that the total NO_x matched the desired concentration but the ratio of NO and NO₂ remained constant.

Models were also run to simulate conditions in the Amazon region, with VOC concentrations adjusted to match observations of isoprene concentrations and OH reactivity in this region. These models were run at a higher isoprene concentration of 5 ppb, and methane concentrations of 100 ppm. (Williams et al., 2016; Pfannerstill et al., 2021; Langford et al., 2022) The latitude and longitude values used corresponded to the city of Manaus and were -3.132° and -60.01° respectively. The time of day was kept at 16:00 local time.

These models are designed for comparison between one another to gain insight into the impact of changes in NO_x and O₃ on organonitrate concentration. The models show the concentrations at steady-state for the provided photolysis conditions, chemistry, and dilution rate, which is in contrast to the constantly changing photolysis and dilution encountered under

100 ambient conditions. This means that chemistry that would occur at other times (e.g. night-time chemistry) does not contribute to the results of these models. Previous work has demonstrated the importance of night-time chemistry for understanding organonitrates, but also that many of the organonitrates produced overnight will decrease in concentrations over the early-morning period to reach low concentrations in the afternoon. (Kenagy et al., 2020; Mayhew et al., 2022) The downstream chemistry of these night-time organonitrates, and other night-time species, will have some impacts on day-time chemistry that are not captured by the models presented here. However, Section 3.1 illustrates that the conclusions made in this paper are applicable to the Beijing afternoon conditions being investigated and that the conclusions are robust to changes in the modelling approach.

2.2 Model Isopleths

Throughout this paper, the model results are investigated through the use of isopleth plots. These plots consist of the steady-state concentration of a species (or another model output such as OH reactivity) in each of the models plotted as a coloured circle at the corresponding position on a set of NO_x - O_3 axes. The colour scale is indicated by a colour bar placed alongside each set of axes and will be a different scale for each plot. A continuous colour gradient is then overlaid on the axes by interpolation over a triangular grid of the model points. 10 contour lines are also drawn over the top of each plot to highlight the contour shape. These lines are equally spaced in the coloured dimension (e.g. species concentration), meaning close vertical lines would correspond to a strong sensitivity to changes in O_3 and close horizontal lines would correspond to a strong sensitivity to changes in NO_x .

Under real-world conditions, the O_3 concentrations will be determined by the non-linear interactions of NO_x and VOCs, which is in contrast to the models where NO_x , O_3 , and VOCs are all constrained. This means that some sections of the model isopleths will be inaccessible. For example, some amount of O_3 will form in the presence of NO_x and VOCs, so occupying the upper-left corner of the isopleths may not be possible outside of the constrained model scenario. Similarly, it may not be possible to map real-world changes to one dimension (such as a decrease in NO_x) onto the isopleth plots without accounting for a change in the other dimension (such as a change in O_3).

2.3 Volatility Calculations

Section 3.6 makes use of the vapour pressure (often expressed as a log value to the base of 10) to investigate the potential contributions to SOA. The UManSysProp facility was used to do this. (Topping et al., 2016) UManSysProp can estimate the vapour pressure of compounds represented as SMILES strings via a range of different group contribution methods. (Barley and Mcfiggans, 2010; O'meara et al., 2014) This work used predictions at 298 K throughout and used the 'evaporation' technique, though sensitivity to all of the available prediction methods is described in Section 3.6.

3 Results and Discussion

3.1 Model Validation

As a test of the ability of the steady-state models to represent conditions present under ambient scenarios, the model results were compared to measurements collected in the summer of 2017 in Beijing. (Shi et al., 2019; Hamilton et al., 2021; Whalley et al., 2021; Reeves et al., 2021; Newland et al., 2021; Mayhew et al., 2022) The NO_x mixing ratios measured in the

afternoon periods in Beijing ranged between 5 ppb and 20 ppb, and O₃ mixing ratios ranged from around 60 ppb to 140 ppb. Isoprene mixing ratios ranged up to around 2 ppb in the afternoon period, hence a typical value of 1 ppb was chosen for the steady state models. The concentration isopleths for inorganic species zoomed in to this representative range of O₃ and NO_x mixing ratios are provided in the supplementary information (Section S1).

Measurements of OH reactivity (k_{OH}) during the afternoon period were between around 10 s⁻¹ and 30 s⁻¹ (Whalley et al., 2021), which the models reproduced at the appropriate NO_x and O₃ mixing ratios by design due to the additional methane included in the model run for this purpose (Figure 4a). The modelled NO₃ reactivity (k_{NO_3}) is around 0.4-1.9 s⁻¹ compared to the estimated value of around 0.5 s⁻¹ presented in Hamilton *et al.* (Figure 4b). (Hamilton et al., 2021). k_{OH} and k_{NO_3} values at a wider range of NO_x and O₃ mixing ratios is provided in Figure S1

In the NO_x-O₃ space corresponding to typical Beijing afternoon conditions, the models show NO mixing ratios of around 0.3-2.8 ppb (Figure 5a, Figure S2a), consistent with the low-NO observations in the afternoon period in Beijing with observed mixing ratios of around 0.25 ppb and 3 ppb. (Newland et al., 2021) The models show NO₃ mixing ratios of 0.4 to 2 ppt (Figure 6a, Figure S3a), which is slightly below the measured NO₃ mixing ratio in the afternoon of around 2 ppt. (Hamilton et al., 2021) The modelled OH concentrations are between 2.5×10⁶ and 6.5×10⁶ molecules cm⁻³ (Figure 6b, Figure S3b), which is slightly below the measured concentrations of around 7.5×10⁶ molecules cm⁻³. HO₂ is generally over predicted with a range between 4.2×10⁸ and 9.1×10⁸ molecules cm⁻³, compared to measurements of around 2.5×10⁸ molecules cm⁻³ (Figure 6c, Figure S3c). (Whalley et al., 2021) This is consistent with previous modelling studies that indicate an over-prediction of HO₂ by models, particularly under the low-NO afternoon conditions being investigated here. (Mayhew et al., 2022; Whalley et al., 2021) Furthermore, models which included an additional sink of HO₂ to bring it in line with measurements resulted in an under-prediction of OH due to the HO_x removed from the system.

A series of sensitivity tests were carried out in order to assess the sensitivity of our conclusions to changes in model parameters. Four different parameters were adjusted: the concentration of isoprene, the concentration of methane, the dilution rate, and the time of day. These sensitivity tests were found to have little impact on the conclusions drawn in this work, and any potential impacts are discussed where required. Further details on tests is provided in the supplementary information (Section S2).

3.2 Mononitrates

The IHN concentration isopleth (Figure 7a) shows a strong similarity to the OH isopleth (Figure 6b), highlighting its rapid formation from the OH oxidation of isoprene and subsequent RO₂ + NO reaction to form the nitrate group (Figure 1). This means that at high O₃ mixing ratios, IHN shows a strong dependence on NO_x, and the dependence on O₃ becomes more significant at lower O₃ mixing ratios.

IPN shows increasing concentrations with increasing O₃ and decreasing NO_x (Figure 7b). This reflects the requirement for low NO concentrations to be present for two reasons. Firstly, high NO₃ concentrations are required to form the INO₂ radical by the reaction of isoprene with NO₃. Secondly, the RO₂+HO₂ reaction is required to form the hydroperoxide group of IPN,

and so lower NO concentrations will reduce competition with the rapid $\text{RO}_2 + \text{NO}$ reaction. Additionally, HO_2 concentrations are highest under low NO_x conditions (Figure 6c), further favouring the $\text{RO}_2 + \text{HO}_2$ reaction.

In contrast to the other nitrated species investigated here, ICN shows two peaks in concentration, one at very low O_3 and the other at very high O_3 (Figure 7c). This is because ICN can be formed from many different routes. Firstly, the abstraction of an H atom from IHN which provides a formation route under lower O_3 conditions, when OH and IHN are both high in concentration. Alternatively, under higher O_3 conditions, ICN can form from the reaction of OH and IPN, or the decomposition of nitrated alkoxy radicals (INO). The result of these multiple peaks is that under moderate NO_x and O_3 conditions, the concentration of ICN is relatively insensitive to changes in both NO_x and O_3 . It is also important to note that the absolute concentrations of ICN predicted to form in these models are very low (the peaks in concentration corresponding to mixing ratios of just over 1 ppt), due to low production rates, which is consistent with low daytime ICN mixing ratios previously identified in Beijing. (Reeves et al., 2021; Mayhew et al., 2022)

Recent work has highlighted species with the formula $\text{C}_4\text{H}_7\text{NO}_5$ as potentially major oxidation products of isoprene. (Tsiligiannis et al., 2022) Consistent with previous modelling studies (Mayhew et al., 2022), these models largely form $\text{C}_4\text{H}_7\text{NO}_5$ from OH-initiated oxidation, meaning the concentration isopleth is similar to that of OH and IHN.

3.3 Nitrated Epoxides

Both INHE and INPE show a similar pattern as IPN in the NO_x - O_3 isopleths (Figure 8a,b), with the highest concentrations occurring at low NO_x and very high O_3 . INPE is reliant on high NO_3 and HO_2 in a similar manner to IPN as the $\text{RO}_2 + \text{HO}_2$ step is still required to form INPE. While HO_2 is not required to form INHE via the alkoxy-epoxidation pathway, the formation of INHE from IPN is the major formation route under lower NO_x conditions. Additionally, the alkoxy-epoxidation pathway to the formation of INHE relies on an RO_2 - RO_2 cross-reaction. This cross reaction will be favoured under low- NO_x -high- O_3 conditions, where NO concentrations will be the lowest, meaning that the competition with the rapid RO_2 -NO reaction is minimal. This requirement for very high O_3 and low NO_x means that we should expect very low concentrations of daytime INHE and INPE under typical urban conditions. This is consistent with modelling of Beijing which showed that while INHE may comprise a large fraction of night-time $\text{C}_5\text{H}_9\text{NO}_5$ compounds, the daytime contribution is very small. (Mayhew et al., 2022)

In contrast, INCE shows reasonably high concentrations under high- O_3 mixing ratios at a range of NO_x mixing ratios. The profile of these concentrations is very similar to the NO_3 isopleth (Figure 6a), and stems from the main formation route to INCE requiring the NO_3 oxidation of isoprene followed by an $\text{RO}_2 + \text{NO}$ reaction step. This formation route shares similarities with the dinitrates discussed in Section 3.4.

3.4 Dinitrates

As previously noted for INCE, Figure 9 shows that the steady-state concentrations of isoprene dinitrate (IDN) and isoprene dinitrooxyepoxide (IDNE) are very similar to the NO_3 concentration isopleth (Figure 6a). This is indicative of the formation route of IDN and IDNE, where an initial NO_3 oxidation is followed by the reaction of the resulting RO_2 with NO to form the

200 second nitrate group (Figure 1 and Figure 3). At any daytime concentration of NO_x where sufficient NO_3 is present to perform the initial oxidation step, there will also be sufficient NO present to rapidly react with the resulting RO_2 . Although the high O_3 mixing ratios observed in Beijing result in low NO concentrations compared to typical daytime concentrations in a polluted megacity, there is still ample NO present to react with peroxy radicals produced by the initial NO_3 oxidation. Figure 9 shows that at each O_3 there is a critical NO_x concentration, above which the concentration of IDN, IDNE, and INCE
205 is almost exclusively controlled by O_3 concentrations. This critical NO_x mixing ratio is reasonably low compared to typical urban NO_x mixing ratios, indicating that the concentration of dinitrates in urban environments may be largely controlled by the O_3 mixing ratios present.

As discussed in Section S2, increasing the total VOC in the model results in a broadening in the NO_x axis of the transition between NO_x and O_3 sensitive regimes for NO_3 , and so the same applies to IDN, IDNE, and INCE. For a fixed ozone
210 concentration, increasing the NO_x from 0 will increase IDN, IDNE, or INCE concentrations due to the increased NO_3 resulting from the increased availability of NO_2 (Figure 10). Then, once the threshold NO_x concentration is reached and NO_3 concentrations are not limited by the availability of NO_x , the concentration becomes controlled by O_3 and HO_2 (Section S2) creating the “hump” in concentration which then stabilises as HO_2 concentrations begin to decrease at high NO_x and the NO_2/NO ratio becomes increasingly controlled by the fixed O_3 concentration. This means that with high VOC
215 concentrations, at a given O_3 concentration, reductions in NO_x will result in increased IDN, IDNE, or ICNE concentrations sooner than under lower VOC conditions.

3.5 Total Organonitrates

By summing the model concentrations for all organonitrates present in the mechanism, an isopleth of total organonitrates was obtained (Figure 11). This shows a band of high organonitrate concentrations at moderate NO_x . At high O_3 , further
220 changes to O_3 have little effect on the total organonitrate concentration. Total organonitrates also become less sensitive to changes in NO_x in this high- O_3 region. This band is the result of organonitrates produced by OH and NO_3 oxidation of isoprene. At low O_3 mixing ratios, the total organonitrates are dominated by OH-initiated species such as IHN (Figure 7a). Conversely, at high O_3 mixing ratios, NO_3 -initiated species such as IDN comprise a larger fraction of total organonitrates (Figure 9a). This is illustrated in the pie charts in Figure 11 which show the organonitrate composition under different NO_x -
225 O_3 regimes.

The composition breakdown also reveals that total isoprene organonitrates are dominated by IHN under most conditions, but this fraction decreases as ozone mixing ratios increase. At higher O_3 , a large fraction of the composition comes from IDN, IDNE, and INCE due to their higher concentrations under high- O_3 conditions (Section 3.3 and Section 3.4). CH_3NO_3 comprises a substantial fraction of total organonitrates in these models. CH_3NO_3 can be formed by the OH oxidation of
230 methane via the methylperoxy radical, and so its concentrations in these models are exaggerated due to the large amounts of methane added to the model. Formation from the OH oxidation of methane comprises the majority of all of the methylperoxy formation in all of the models, excluding formation from the reversible decomposition of methane peroxyxynitrate ($\text{CH}_3\text{O}_2\text{NO}_2$) which is balanced by the opposing formation reaction. $\text{CH}_2\text{NO}_2\text{OOH}$ is also listed in Figure 11.

235 CH₂NO₂OOH is formed from the products of isoprene ozonolysis, explaining the higher concentrations under high-O₃ conditions. There are no chemical losses in the mechanism for CH₂NO₂OOH, which likely explains the high contribution to total organonitrates. The remaining portion of “other” organonitrates corresponds to a wide range of species, none of which contribute more than 6% to the total organonitrate sum in any models.

240 As noted in Section S2, changing the VOC concentration effects the position in NO_x-O₃ space where the maximum organonitrate concentrations are observed. In the case of total organonitrates, decreasing the total VOC concentration results in the band of high concentrations moving to lower NO_x. Figure S7 and Figure S8 show that with lower methane concentrations in the model, the peak organonitrate concentrations occur at around 12 ppb of NO_x whereas this increases to around 25 ppb of NO_x in the high methane case. The peak organonitrate concentrations at each of these NO_x concentrations are similar in each of these sets of model runs.

3.6 Volatility Assessment

245 One of the major motivations for studying isoprene nitrates is their potential to contribute to secondary organic aerosol (SOA) by condensation or reactive uptake to existing particles. While the highest concentration species such as IHN and IDN may be most significant when considering the role of isoprene nitrates as NO_x reservoirs, low concentration species can be much more important for SOA formation if they are of a sufficiently low volatility. As an estimation of the impact of changing NO_x and O₃ on particle-phase processes, the log of the vapour pressure was estimated for each organonitrate in the mechanism based on the species’ structure using UManSysProp.(Topping et al., 2016) As a measure of a compound’s volatility, a lower vapour pressure value corresponds to a less volatile compound which will more readily partition into existing particles. This volatility-based approach does not account for potential reactive uptake which is likely to be important for the epoxide species previously discussed. Furthermore, the hydrolysis of organonitrates, particularly tertiary nitrates, may reduce particle-phase concentrations.(Vasquez et al., 2020)

255 Figure 12 shows the total organonitrate plot normalised to the vapour pressure value for each compound, which gives an estimation of the contribution of organonitrate uptake to SOA at each NO_x and O₃ mixing ratio. Since the predicted vapour pressures range over 10 orders of magnitude, lower volatility species can have a large effect on SOA formation despite their much lower concentration. The lowest vapour pressures predicted here are for the two MCM species NC524NO₃ and NC524OOH. These two compounds comprise almost 100% of the normalised concentration in Figure 12 under all NO_x and O₃ conditions, and their individual concentration profiles can be seen in Figure 13. The concentration isopleths for the 15 lowest volatility compounds are shown in Figure S17. Many of these species show profiles similar to that of NC524OOH, with the highest concentrations occurring at low urban NO_x concentrations.

265 According to Figure 12, reductions in NO_x from typical urban conditions would result in higher normalised concentrations of organonitrates, meaning the contribution of isoprene nitrates to SOA may increase with decreasing NO_x until very low urban NO_x conditions are met. However, it is important to note the difficulty in representing the lowest volatility species in the isoprene oxidation mechanism. Many of these species are the product of multiple oxidation steps with large uncertainties

surrounding their rates of formation. Additionally, many of the lowest volatility species do not contain any chemical losses in the mechanism due to a lack of information on their reactions.

270 The low predicted volatilities of NC524NO₃ and NC524OOH are the result of the many functional groups present in the molecules. Similarly oxidised species could be described as highly oxidised molecules (HOMs). (Bianchi et al., 2019) The chemistry of HOMs is not currently well represented in many mechanisms due to their varied autooxidation formation pathways. For example, the profile of NC524OOH concentrations in Figure 13b results from the requirement of HO₂ to form the hydroperoxide group, hence the profile is similar to that of HO₂. If an RO₂ H-shift formation pathway to NC524OOH, or similar HOMs, were included in the mechanism, then this might alter the profile in Figure 12. (Vereecken and Nozière, 275 2020) It should be expected that the formation of HOMs would be sensitive to changes in ozone as the lower NO concentrations at higher ozone will reduce the competition of the RO₂+NO pathway with the RO₂ autooxidation reactions that form HOMs. Inclusion of improved autooxidation chemistry in the mechanisms would also increase the number of low volatility compounds produced from the oxidation of isoprene. There is also the potential for the oxidation products of night-time species to be low volatility compounds that would contribute to SOA but would not be captured by these models which 280 represent the steady-state concentration of organonitrates at 16:00, without the contribution of chemistry occurring at other times of the day.

Figure S16 shows that the results presented here are reasonably insensitive to the choice of vapour pressure and boiling point prediction methods selected within UManSysProp. Section S3 also outlines the results using an alternative volatility estimation method, making use of only the molecular formula of each compound.

285 3.7 Application to Less Polluted Environments

In order to test the investigation of less polluted environments, a series of models were run at a range of lower NO_x and O₃ mixing ratios. Measurements collected in the amazon rainforest were taken as an example of an unpolluted environment, and the model was adjusted to match typical isoprene mixing ratios and OH reactivity observed in this environment. The results from these models are presented in the supplementary information (Section S5).

290 The reduced NO_x and O₃ mixing ratios used in these models mean that, despite the changes to isoprene and methane concentrations, they correspond well to higher resolution models of the low NO_x and O₃ portions of the Beijing models. Figure S19 shows that the total organonitrates in the Amazon models are sensitive to changes in NO_x, with increasing ozone slightly reducing total organonitrates.

As discussed in the introduction, IEPOX is one of the major precursors of isoprene SOA, particularly under low-NO_x 295 conditions where the IEPOX precursor, ISOPPOOH, can form from oxidation by OH and further reaction with HO₂. This dependence on HO₂ means that the amazon models predict increasing concentrations of IEPOX as NO_x is increased from close to 0, regardless of the O₃ concentration (Figure 14b). This is in agreement with findings from Shrivastava et al. who found increases in isoprene SOA resulting from increases in NO_x and O₃ from an urban plume (Shrivastava et al., 2019) The increased SOA could be further explained by the increases in nitrated epoxides and dinitrated species predicted on increasing 300 both NO_x and O₃ (Figure S19).

Methyl vinyl ketone (MVK) and methacrolein (MACR) are also often of interest in isoprene oxidation, particularly in pristine environments such as the Amazon where the production of MVK and MACR relies on the presence of NO. (Langford et al., 2022) This is illustrated in Figure 14d, whereas Figure 14c illustrates that the abundance of NO under typical urban conditions means that the MVK+MACR concentrations in the Beijing models are dependent on OH concentrations.

4 Conclusions

The work presented here illustrates that each isoprene nitrate species will have a different NO_x-O₃ regime in which maximum concentrations will be produced during the afternoon period. For example, the facile formation of IHN from OH oxidation means that daytime concentrations are largely dictated by the concentration of OH. Alternatively, the concentrations of species such as IDN, IDNE, and ICN are largely dictated by the available daytime NO₃ as the reaction of RO₂ with NO is very rapid, even under low urban NO_x conditions. Finally, IPN, INHE, and INPE only show the highest concentrations under low-NO_x-high-O₃ conditions due to their increased formation under high NO₃ concentrations and their requirement for low-NO_x to avoid competition with the RO₂+NO reaction pathway.

The fact that the concentrations of different organonitrates will respond differently to changes in NO_x and O₃ will have implications for those considering pathways to reducing the concentrations of organonitrates in the atmosphere. The work presented here indicates that reductions in NO_x may not reduce total organonitrate concentrations until low urban NO_x conditions are met and that, for many of the species resulting from the daytime NO₃ oxidation of isoprene, organonitrate concentrations may be much more sensitive to changes in O₃ than in NO_x. Additionally, accounting for the volatility of the organonitrates can have very large impacts, and the models presented here are dominated by a small number of low volatility compounds. An improved representation of late-stage oxidation and autooxidation is likely to improve the ability to predict the effect of changing O₃ and NO_x on SOA formation. It is important to note that the simplified models presented here represent the formation of day-time isoprene organonitrates at 16:00 and will not capture the effect of organonitrates produced during the night-time or those produced from the oxidation of night-time products or other VOCs.

As efforts are made to reduce NO_x, VOC, and O₃ concentrations around the world, care should be taken to ensure that the non-linearity of responses to changes does not result in unintended increases in important SOA precursors. For example, previous work has indicated that Beijing occupies a VOC-limited regime with respect to O₃ formation and that decreasing NO_x concentrations without a concurrent decrease in VOC concentrations would result in increased O₃. (Wei et al., 2019; Ren et al., 2021) Figure 12 suggests that many of the lowest volatility daytime isoprene organonitrates may form in higher concentrations under higher O₃ and lower NO_x. Furthermore, INHE, IDNE, INPE, and INCE all favour formation under high-O₃ conditions and may be subject to reactive uptake to the particle phase. This may be further compounded or mitigated with changing VOC concentrations due to the impact on the organonitrate isopleths as well as the non-linear behaviour of O₃ with changing NO_x and VOC.

Future chamber and field studies could validate the findings from this work by making more comprehensive observations of total and speciated organonitrates under different NO_x, O₃, and VOC concentrations. The comparative nature of these isopleth plots mean that the organonitrate measurement would not necessarily need to be calibrated, provided that the instrument response to specific organonitrates can be assumed to be constant. This makes long-term measurements made with iodide chemical ionisation mass spectrometry (I-CIMS) a promising dataset as I-CIMS is very sensitive to these multifunctional compounds, but calibration is often difficult. (Mayhew et al., 2022; Lee et al., 2014)

5 Competing interests

The authors declare that they have no conflict of interest.

6 Acknowledgements

This project was undertaken on the Viking Cluster, which is a high performance compute facility provided by the University of York. We are grateful for computational support from the University of York High Performance Computing service, Viking and the Research Computing team.

7 Financial Support

This work was supported by the Leeds-York-Hull Natural Environment Research Council (NERC) Doctoral Training Partnership (DTP) Panorama under grant NE/S007458/1.

8 References

- Barley, M. H. and McFiggans, G.: The critical assessment of vapour pressure estimation methods for use in modelling the formation of atmospheric organic aerosol, *Atmospheric Chemistry and Physics*, 10, 749-767, 10.5194/acp-10-749-2010, 2010.
- Bates, K. H. and Jacob, D. J.: A new model mechanism for atmospheric oxidation of isoprene: global effects on oxidants, nitrogen oxides, organic products, and secondary organic aerosol, *Atmospheric Chemistry and Physics*, 19, 9613-9640, 10.5194/acp-19-9613-2019, 2019.
- Bianchi, F., Kurtén, T., Riva, M., Mohr, C., Rissanen, M. P., Roldin, P., Berndt, T., Crouse, J. D., Wennberg, P. O., Mentel, T. F., Wildt, J., Junninen, H., Jokinen, T., Kulmala, M., Worsnop, D. R., Thornton, J. A., Donahue, N., Kjaergaard, H. G., and Ehn, M.: Highly Oxygenated Organic Molecules (HOM) from Gas-Phase Autoxidation Involving Peroxy Radicals: A Key Contributor to Atmospheric Aerosol, *Chemical Reviews*, 119, 3472-3509, 10.1021/acs.chemrev.8b00395, 2019.
- Brown, S. S., Osthoff, H. D., Stark, H., Dubé, W. P., Ryerson, T. B., Warneke, C., de Gouw, J. A., Wollny, A. G., Parrish, D. D., Fehsenfeld, F. C., and Ravishankara, A. R.: Aircraft observations of daytime NO₃ and N₂O₅ and their implications for tropospheric chemistry, *Journal of Photochemistry and Photobiology A: Chemistry*, 176, 270-278, 10.1016/j.jphotochem.2005.10.004, 2005.
- Carlsson, P. T. M., Vereecken, L., Novelli, A., Bernard, F., Brown, S. S., Brownwood, B., Cho, C., Crowley, J. N., Dewald, P., Edwards, P. M., Friedrich, N., Fry, J. L., Hallquist, M., Hantschke, L., Hohaus, T., Kang, S., Liebmann, J., Mayhew, A.

- W., Mentel, T., Reimer, D., Rohrer, F., Shenolikar, J., Tillmann, R., Tsiligiannis, E., Wu, R., Wahner, A., Kiendler-Scharr, A., and Fuchs, H.: Comparison of isoprene chemical mechanisms at atmospheric night-time conditions in chamber experiments: Evidence of hydroperoxy aldehydes and epoxy products from NO₃ oxidation, *Atmos. Chem. Phys.*, 10.5194/acp-23-3147-2023, 2023.
- 370 Edwards, P. M., Young, C. J., Aikin, K., Degouw, J., Dubé, W. P., Geiger, F., Gilman, J., Helmig, D., Holloway, J. S., Kercher, J., Lerner, B., Martin, R., McLaren, R., Parrish, D. D., Peischl, J., Roberts, J. M., Ryerson, T. B., Thornton, J., Warneke, C., Williams, E. J., and Brown, S. S.: Ozone photochemistry in an oil and natural gas extraction region during winter: simulations of a snow-free season in the Uintah Basin, Utah, *Atmospheric Chemistry and Physics*, 13, 8955-8971, 10.5194/acp-13-8955-2013, 2013.
- 375 Edwards, P. M., Brown, S. S., Roberts, J. M., Ahmadov, R., Banta, R. M., Degouw, J. A., Dubé, W. P., Field, R. A., Flynn, J. H., Gilman, J. B., Graus, M., Helmig, D., Koss, A., Langford, A. O., Lefer, B. L., Lerner, B. M., Li, R., Li, S.-M., McKeen, S. A., Murphy, S. M., Parrish, D. D., Senff, C. J., Soltis, J., Stutz, J., Sweeney, C., Thompson, C. R., Trainer, M. K., Tsai, C., Veres, P. R., Washenfelder, R. A., Warneke, C., Wild, R. J., Young, C. J., Yuan, B., and Zamora, R.: High winter ozone pollution from carbonyl photolysis in an oil and gas basin, *Nature*, 514, 351-354, 10.1038/nature13767, 2014.
- 380 Emmerson, K. L. and Evans, M. J.: Comparison of tropospheric gas-phase chemistry schemes for use within global models, *Atmos. Chem. Phys.*, 9, 1831-1845, 10.5194/acp-9-1831-2009, 2009.
- Forkel, R., Klemm, O., Graus, M., Rappenglück, B., Stockwell, W. R., Grabmer, W., Held, A., Hansel, A., and Steinbrecher, R.: Trace gas exchange and gas phase chemistry in a Norway spruce forest: A study with a coupled 1-dimensional canopy atmospheric chemistry emission model, *Atmospheric Environment*, 40, 28-42, 10.1016/j.atmosenv.2005.11.070, 2006.
- 385 Foulds, A., Khan, M. A. H., Bannan, T. J., Percival, C. J., Lowenberg, M. H., and Shallcross, D. E.: Abundance of NO₃ Derived Organo-Nitrates and Their Importance in the Atmosphere, *Atmosphere*, 12, 10.3390/atmos12111381, 2021.
- Geyer, A.: Direct observations of daytime NO₃: Implications for urban boundary layer chemistry, *Journal of Geophysical Research*, 108, 10.1029/2002jd002967, 2003.
- Guenther, A., Karl, T., Harley, P., Wiedinmyer, C., Palmer, P. I., and Geron, C.: Estimates of global terrestrial isoprene emissions using MEGAN (Model of Emissions of Gases and Aerosols from Nature), *Atmospheric Chemistry and Physics*, 6, 3181-3210, 10.5194/acp-6-3181-2006, 2006.
- Hallquist, M., Wenger, J. C., Baltensperger, U., Rudich, Y., Simpson, D., Claeys, M., Dommen, J., Donahue, N. M., George, C., Goldstein, a. H., Hamilton, J. F., Herrmann, H., Hoffmann, T., Iinuma, Y., Jang, M., Jenkin, M. E., Jimenez, J. L., Kiendler-Scharr, a., Maenhaut, W., McFiggans, G., Mentel, T. F., Monod, a., Prévôt, a. S. H., Seinfeld, J. H., Surratt, J. D., Szmigielski, R., and Wildt, J.: The formation, properties and impact of secondary organic aerosol: current and emerging issues, *Atmos. Chem. Phys.*, 9, 5155-5236, 10.5194/acp-9-5155-2009, 2009.
- 395 Hamilton, J. F., Bryant, D. J., Edwards, P. M., Ouyang, B., Bannan, T. J., Mehra, A., Mayhew, A. W., Hopkins, J. R., Dunmore, R. E., Squires, F. A., Lee, J. D., Newland, M. J., Worrall, S. D., Bacak, A., Coe, H., Percival, C., Whalley, L. K., Heard, D. E., Slater, E. J., Jones, R. L., Cui, T., Surratt, J. D., Reeves, C. E., Mills, G. P., Grimmond, S., Sun, Y., Xu, W., Shi, Z., and Rickard, A. R.: Key Role of NO₃ Radicals in the Production of Isoprene Nitrates and Nitrooxyorganosulfates in Beijing, *Environ Sci Technol*, 55, 842-853, 10.1021/acs.est.0c05689, 2021.
- 400 Hu, X.-M., Fuentes, J. D., Toohey, D., and Wang, D.: Chemical processing within and above a loblolly pine forest in North Carolina, USA, *Journal of Atmospheric Chemistry*, 72, 235-259, 10.1007/s10874-013-9276-3, 2013.
- Jenkin, M. E., Young, J. C., and Rickard, A. R.: The MCM v3.3.1 degradation scheme for isoprene, *Atmospheric Chemistry and Physics*, 15, 11433-11459, 10.5194/acp-15-11433-2015, 2015.
- 405 Kenagy, H. S., Sparks, T. L., Wooldridge, P. J., Weinheimer, A. J., Ryerson, T. B., Blake, D. R., Hornbrook, R. S., Apel, E. C., and Cohen, R. C.: Evidence of Nighttime Production of Organic Nitrates During SEAC 4 RS, FRAPPÉ, and KORUS-AQ, *Geophysical Research Letters*, 47, 10.1029/2020gl087860, 2020.
- Khan, M. A. H., Morris, W. C., Watson, L. A., Galloway, M., Hamer, P. D., Shallcross, B. M. A., Percival, C. J., and Shallcross, D. E.: Estimation of Daytime NO₃ Radical Levels in the UK Urban Atmosphere Using the Steady State Approximation Method, *Advances in Meteorology*, 2015, 1-9, 10.1155/2015/294069, 2015.
- 410 Langford, B., House, E., Valach, A., Hewitt, C. N., Artaxo, P., Barkley, M. P., Brito, J., Carnell, E., Davison, B., MacKenzie, A. R., Marais, E. A., Newland, M. J., Rickard, A. R., Shaw, M. D., Yáñez-Serrano, A. M., and Nemitz, E.: Seasonality of isoprene emissions and oxidation products above the remote Amazon, *Environmental Science: Atmospheres*, 2, 230-240, 10.1039/d1ea00057h, 2022.

- Lee, B. H., Lopez-Hilfiker, F. D., Mohr, C., Kurtén, T., Worsnop, D. R., and Thornton, J. A.: An Iodide-Adduct High-Resolution Time-of-Flight Chemical-Ionization Mass Spectrometer: Application to Atmospheric Inorganic and Organic Compounds, *Environmental Science & Technology*, 48, 6309-6317, 10.1021/es500362a, 2014.
- 420 Mayhew, A. W., Lee, B. H., Thornton, J. A., Bannan, T. J., Brean, J., Hopkins, J. R., Lee, J. D., Nelson, B. S., Percival, C., Rickard, A. R., Shaw, M. D., Edwards, P. M., and Hamilton, J. F.: Evaluation of isoprene nitrate chemistry in detailed chemical mechanisms, *Atmospheric Chemistry and Physics*, 22, 14783-14798, 10.5194/acp-22-14783-2022, 2022.
- 425 Mermet, K., Perraudin, E., Dusanter, S., Sauvage, S., Leonardis, T., Flaud, P. M., Bsaibes, S., Kammer, J., Michoud, V., Gratien, A., Cirtog, M., Al Ajami, M., Truong, F., Batut, S., Hecquet, C., Doussin, J. F., Schoemaeker, C., Gros, V., Locoge, N., and Villenave, E.: Atmospheric reactivity of biogenic volatile organic compounds in a maritime pine forest during the LANDEX episode 1 field campaign, *Sci Total Environ*, 756, 144129, 10.1016/j.scitotenv.2020.144129, 2021.
- 430 Newland, M. J., Bryant, D. J., Dunmore, R. E., Bannan, T. J., Acton, W. J. F., Langford, B., Hopkins, J. R., Squires, F. A., Dixon, W., Drysdale, W. S., Ivatt, P. D., Evans, M. J., Edwards, P. M., Whalley, L. K., Heard, D. E., Slater, E. J., Woodward-Massey, R., Ye, C., Mehra, A., Worrall, S. D., Bacak, A., Coe, H., Percival, C. J., Hewitt, C. N., Lee, J. D., Cui, T., Surratt, J. D., Wang, X., Lewis, A. C., Rickard, A. R., and Hamilton, J. F.: Low-NO atmospheric oxidation pathways in a polluted megacity, *Atmospheric Chemistry and Physics*, 21, 1613-1625, 10.5194/acp-21-1613-2021, 2021.
- O'Meara, S., Booth, A. M., Barley, M. H., Topping, D., and McFiggans, G.: An assessment of vapour pressure estimation methods, *Phys. Chem. Chem. Phys.*, 16, 19453-19469, 10.1039/c4cp00857j, 2014.
- Osthoff, H. D., Sommariva, R., Baynard, T., Pettersson, A., Williams, E. J., Lerner, B. M., Roberts, J. M., Stark, H., Goldan, P. D., Kuster, W. C., Bates, T. S., Coffman, D., Ravishankara, A. R., and Brown, S. S.: Observation of daytime N₂O₅ in the marine boundary layer during New England Air Quality Study-Intercontinental Transport and Chemical Transformation 2004, *Journal of Geophysical Research: Atmospheres*, 111, 10.1029/2006jd007593, 2006.
- 435 Palmer, P. I., Marvin, M. R., Siddans, R., Kerridge, B. J., and Moore, D. P.: Nocturnal survival of isoprene linked to formation of upper tropospheric organic aerosol, *Science*, 375, 562-566, 10.1126/science.abg4506, 2022.
- 440 Paulot, F., Crouse, J. D., Kjaergaard, H. G., Kürten, A., St Clair, J. M., Seinfeld, J. H., and Wennberg, P. O.: Unexpected Epoxide Formation in the Gas-Phase Photooxidation of Isoprene, *Science*, 325, 730-733, 10.1126/science.1172910, 2009.
- Pfannerstill, E. Y., Reijrink, N. G., Edtbauer, A., Ringsdorf, A., Zannoni, N., Araújo, A., Ditas, F., Holanda, B. A., Sá, M. O., Tsokankunku, A., Walter, D., Wolff, S., Lavrič, J. V., Pöhlker, C., Sörgel, M., and Williams, J.: Total OH reactivity over the Amazon rainforest: variability with temperature, wind, rain, altitude, time of day, season, and an overall budget closure, *Atmospheric Chemistry and Physics*, 21, 6231-6256, 10.5194/acp-21-6231-2021, 2021.
- 445 Pye, H. O., Luecken, D. J., Xu, L., Boyd, C. M., Ng, N. L., Baker, K. R., Ayres, B. R., Bash, J. O., Baumann, K., Carter, W. P., Edgerton, E., Fry, J. L., Hutzell, W. T., Schwede, D. B., and Shepson, P. B.: Modeling the Current and Future Roles of Particulate Organic Nitrates in the Southeastern United States, *Environ Sci Technol*, 49, 14195-14203, 10.1021/acs.est.5b03738, 2015.
- 450 Reeves, C. E., Mills, G. P., Whalley, L. K., Acton, W. J. F., Bloss, W. J., Crilley, L. R., Grimmond, S., Heard, D. E., Hewitt, C. N., Hopkins, J. R., Kotthaus, S., Kramer, L. J., Jones, R. L., Lee, J. D., Liu, Y., Ouyang, B., Slater, E., Squires, F., Wang, X., Woodward-Massey, R., and Ye, C.: Observations of speciated isoprene nitrates in Beijing: implications for isoprene chemistry, *Atmospheric Chemistry and Physics*, 21, 6315-6330, 10.5194/acp-21-6315-2021, 2021.
- 455 Ren, J., Hao, Y., Simayi, M., Shi, Y., and Xie, S.: Spatiotemporal variation of surface ozone and its causes in Beijing, China since 2014, *Atmospheric Environment*, 260, 10.1016/j.atmosenv.2021.118556, 2021.
- Schwantes, R. H., Charan, S. M., Bates, K. H., Huang, Y., Nguyen, T. B., Mai, H., Kong, W., Flagan, R. C., and Seinfeld, J. H.: Low-volatility compounds contribute significantly to isoprene secondary organic aerosol (SOA) under high-NO_x conditions, *Atmospheric Chemistry and Physics*, 19, 7255-7278, 10.5194/acp-19-7255-2019, 2019.
- 460 Schwantes, R. H., Teng, A. P., Nguyen, T. B., Coggon, M. M., Crouse, J. D., St. Clair, J. M., Zhang, X., Schilling, K. A., Seinfeld, J. H., and Wennberg, P. O.: Isoprene NO₃ Oxidation Products from the RO₂ + HO₂ Pathway, *Journal of Physical Chemistry A*, 119, 10158-10171, 10.1021/acs.jpca.5b06355, 2015.
- Schwantes, R. H., Emmons, L. K., Orlando, J. J., Barth, M. C., Tyndall, G. S., Hall, S. R., Ullmann, K., St. Clair, J. M., Blake, D. R., Wisthaler, A., and Bui, T. P. V.: Comprehensive isoprene and terpene gas-phase chemistry improves simulated surface ozone in the southeastern US, *Atmospheric Chemistry and Physics*, 20, 3739-3776, 10.5194/acp-20-3739-2020, 2020.

- 465 Shi, Z., Vu, T., Kotthaus, S., Harrison, R. M., Grimmond, S., Yue, S., Zhu, T., Lee, J., Han, Y., Demuzere, M., Dunmore, R. E., Ren, L., Liu, D., Wang, Y., Wild, O., Allan, J., Acton, W. J., Barlow, J., Barratt, B., Beddows, D., Bloss, W. J., Calzolari, G., Carruthers, D., Carslaw, D. C., Chan, Q., Chatzidiakou, L., Chen, Y., Crilley, L., Coe, H., Dai, T., Doherty, R., Du an, F., Fu, P., Ge, B., Ge, M., Guan, D., Hamilton, J. F., He, K., Heal, M., Heard, D., Hewitt, C. N., Hollaway, M., Hu, M., Ji, D., Jiang, X., Jones, R., Kalberer, M., Kelly, F. J., Kramer, L., Langford, B., Lin, C., Lewis, A. C., Li, J., Li, W., Liu, H., Liu, J.,
- 470 Loh, M., Lu, K., Lucarelli, F., Mann, G., McFiggans, G., Miller, M. R., Mills, G., Monk, P., Nemitz, E., O'Connor, F., Ouyang, B., Palmer, P. I., Percival, C., Popoola, O., Reeves, C., Rickard, A. R., Shao, L., Shi, G., Spracklen, D., Stevenson, D., Sun, Y., Sun, Z., Tao, S., Tong, S., Wang, Q., Wang, W., Wang, X., Wang, X., Wang, Z., Wei, L., Whalley, L., Wu, X., Wu, Z., Xie, P., Yang, F., Zhang, Q., Zhang, Y., Zhang, Y., and Zheng, M.: Introduction to the special issue “In-depth study of air pollution sources and processes within Beijing and its surrounding region (APHH-Beijing)”, *Atmospheric Chemistry and Physics*, 19, 7519-7546, 10.5194/acp-19-7519-2019, 2019.
- 475 Shrivastava, M., Andreae, M. O., Artaxo, P., Barbosa, H. M. J., Berg, L. K., Brito, J., Ching, J., Easter, R. C., Fan, J., Fast, J. D., Feng, Z., Fuentes, J. D., Glasius, M., Goldstein, A. H., Alves, E. G., Gomes, H., Gu, D., Guenther, A., Jathar, S. H., Kim, S., Liu, Y., Lou, S., Martin, S. T., McNeill, V. F., Medeiros, A., De Sá, S. S., Shilling, J. E., Springston, S. R., Souza, R. A. F., Thornton, J. A., Isaacman-Vanwertz, G., Yee, L. D., Ynoue, R., Zaveri, R. A., Zelenyuk, A., and Zhao, C.: Urban
- 480 pollution greatly enhances formation of natural aerosols over the Amazon rainforest, *Nature Communications*, 10, 10.1038/s41467-019-08909-4, 2019.
- Sommariva, R., Cox, S., Martin, C., Borońska, K., Young, J., Jimack, P., Pilling, M. J., Matthaios, V. N., Newland, M. J., Panagi, M., Bloss, W. J., Monks, P. S., and Rickard, A. R.: AtChem, an open source box-model for the Master Chemical Mechanism, *Geoscientific Model Development*, 10.5194/gmd-2019-192, 2019.
- 485 Surratt, J. D., Chan, A. W. H., Eddingsaas, N. C., Chan, M., Loza, C. L., Kwan, A. J., Hersey, S. P., Flagan, R. C., Wennberg, P. O., and Seinfeld, J. H.: Reactive intermediates revealed in secondary organic aerosol formation from isoprene, *Proceedings of the National Academy of Sciences*, 107, 6640-6645, 10.1073/pnas.0911114107, 2010.
- Topping, D., Barley, M., Bane, M. K., Higham, N., Aumont, B., Dingle, N., and McFiggans, G.: UManSysProp v1.0: an online and open-source facility for molecular property prediction and atmospheric aerosol calculations, *Geoscientific Model Development*, 9, 899-914, 10.5281/zenodo.45143, 2016.
- 490 Tsiligiannis, E., Wu, R., Lee, B. H., Salvador, C. M., Priestley, M., Carlsson, P. T. M., Kang, S., Novelli, A., Vereecken, L., Fuchs, H., Mayhew, A. W., Hamilton, J. F., Edwards, P. M., Fry, J. L., Brownwood, B., Brown, S. S., Wild, R. J., Bannan, T. J., Coe, H., Allan, J., Surratt, J. D., Bacak, A., Artaxo, P., Percival, C., Guo, S., Hu, M., Wang, T., Mentel, T. F., Thornton, J. A., and Hallquist, M.: A Four Carbon Organonitrate as a Significant Product of Secondary Isoprene Chemistry, *Geophysical Research Letters*, 49, 10.1029/2021gl097366, 2022.
- 495 Vasquez, K. T., Crouse, J. D., Schulze, B. C., Bates, K. H., Teng, A. P., Xu, L., Allen, H. M., and Wennberg, P. O.: Rapid hydrolysis of tertiary isoprene nitrate efficiently removes NO_x from the atmosphere, *Proceedings of the National Academy of Sciences*, 117, 33011-33016, 10.1073/pnas.2017442117, 2020.
- Vereecken, L. and Nozière, B.: H migration in peroxy radicals under atmospheric conditions, *Atmospheric Chemistry and Physics*, 20, 7429-7458, 10.5194/acp-20-7429-2020, 2020.
- 500 Vereecken, L., Carlsson, P. T. M., Novelli, A., Bernard, F., Brown, S. S., Cho, C., Crowley, J. N., Fuchs, H., Mellouki, W., Reimer, D., Shenolikar, J., Tillmann, R., Zhou, L., Kiendler-Scharr, A., and Wahner, A.: Theoretical and experimental study of peroxy and alkoxy radicals in the NO₃-initiated oxidation of isoprene, *Phys Chem Chem Phys*, 23, 5496-5515, 10.1039/d0cp06267g, 2021.
- 505 Wang, H., Chen, X., Lu, K., Hu, R., Li, Z., Wang, H., Ma, X., Yang, X., Chen, S., Dong, H., Liu, Y., Fang, X., Zeng, L., Hu, M., and Zhang, Y.: NO₃ and N₂O₅ chemistry at a suburban site during the EXPLORE-YRD campaign in 2018, *Atmospheric Environment*, 224, 10.1016/j.atmosenv.2019.117180, 2020.
- Wei, W., Li, Y., Ren, Y., Cheng, S., and Han, L.: Sensitivity of summer ozone to precursor emission change over Beijing during 2010–2015: A WRF-Chem modeling study, *Atmospheric Environment*, 218, 10.1016/j.atmosenv.2019.116984, 2019.
- 510 Wennberg, P. O., Bates, K. H., Crouse, J. D., Dodson, L. G., McVay, R. C., Mertens, L. A., Nguyen, T. B., Praske, E., Schwantes, R. H., Smarte, M. D., St Clair, J. M., Teng, A. P., Zhang, X., and Seinfeld, J. H.: Gas-Phase Reactions of Isoprene and Its Major Oxidation Products, *Chemical Reviews*, 118, 3337-3390, 10.1021/acs.chemrev.7b00439, 2018.
- Whalley, L. K., Slater, E. J., Woodward-Massey, R., Ye, C., Lee, J. D., Squires, F., Hopkins, J. R., Dunmore, R. E., Shaw, M., Hamilton, J. F., Lewis, A. C., Mehra, A., Worrall, S. D., Bacak, A., Bannan, T. J., Coe, H., Percival, C. J., Ouyang, B.,

- 515 Jones, R. L., Crilley, L. R., Kramer, L. J., Bloss, W. J., Vu, T., Kotthaus, S., Grimmond, S., Sun, Y., Xu, W., Yue, S., Ren, L., Acton, W. J. F., Hewitt, C. N., Wang, X., Fu, P., and Heard, D. E.: Evaluating the sensitivity of radical chemistry and ozone formation to ambient VOCs and NO_x in Beijing, *Atmospheric Chemistry and Physics*, 21, 2125-2147, 10.5194/acp-21-2125-2021, 2021.
- Williams, J., Keßel, S. U., Nölscher, A. C., Yang, Y., Lee, Y., Yáñez-Serrano, A. M., Wolff, S., Kesselmeier, J., Klüpfel, T.,
 520 Lelieveld, J., and Shao, M.: Opposite OH reactivity and ozone cycles in the Amazon rainforest and megacity Beijing: Subversion of biospheric oxidant control by anthropogenic emissions, *Atmospheric Environment*, 125, 112-118, 10.1016/j.atmosenv.2015.11.007, 2016.
- Xiong, F., McAvey, K. M., Pratt, K. A., Groff, C. J., Hostetler, M. A., Lipton, M. A., Starn, T. K., Seeley, J. V., Bertman, S. B., Teng, A. P., Crouse, J. D., Nguyen, T. B., Wennberg, P. O., Misztal, P. K., Goldstein, A. H., Guenther, A. B., Koss, A. R., Olson, K. F., De Gouw, J. A., Baumann, K., Edgerton, E. S., Feiner, P. A., Zhang, L., Miller, D. O., Brune, W. H., and Shepson, P. B.: Observation of isoprene hydroxynitrates in the southeastern United States and implications for the fate of NO_x, *Atmospheric Chemistry and Physics*, 15, 11257-11272, 10.5194/acp-15-11257-2015, 2015.
 525 R., Olson, K. F., De Gouw, J. A., Baumann, K., Edgerton, E. S., Feiner, P. A., Zhang, L., Miller, D. O., Brune, W. H., and Shepson, P. B.: Observation of isoprene hydroxynitrates in the southeastern United States and implications for the fate of NO_x, *Atmospheric Chemistry and Physics*, 15, 11257-11272, 10.5194/acp-15-11257-2015, 2015.
- Xue, L., Gu, R., Wang, T., Wang, X., Saunders, S., Blake, D., Louie, P. K. K., Luk, C. W. Y., Simpson, I., Xu, Z., Wang, Z., Gao, Y., Lee, S., Mellouki, A., and Wang, W.: Oxidative capacity and radical chemistry in the polluted atmosphere of Hong Kong and Pearl River Delta region: analysis of a severe photochemical smog episode, *Atmospheric Chemistry and Physics*,
 530 Kong and Pearl River Delta region: analysis of a severe photochemical smog episode, *Atmospheric Chemistry and Physics*, 16, 9891-9903, 10.5194/acp-16-9891-2016, 2016.

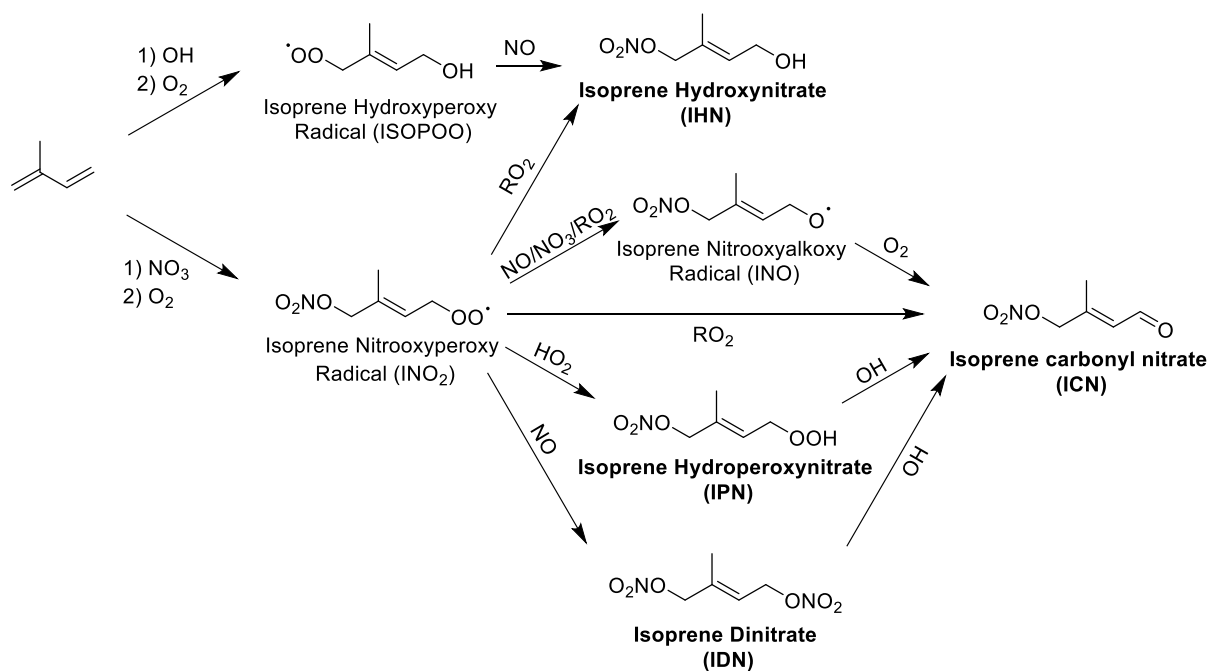
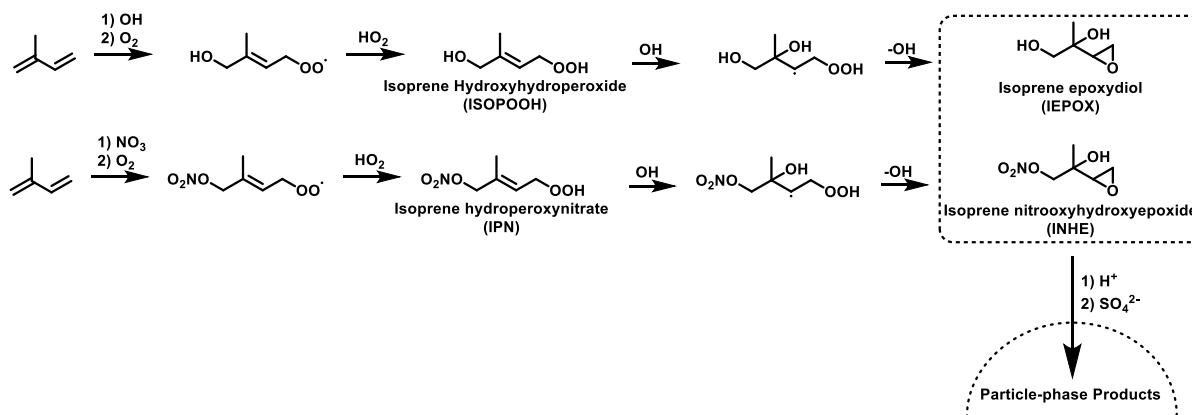
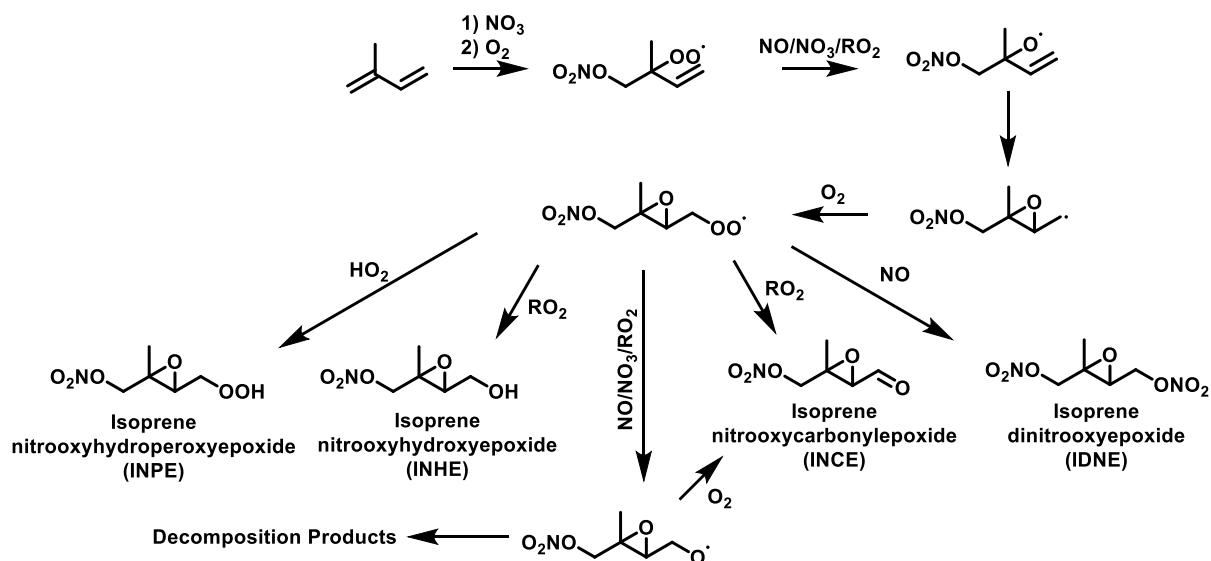


Figure 1. Formation routes to form IHN, ICN, IPN, and IDN from the OH- and NO₃-initiated oxidation of isoprene. Additional isomers and reaction pathways have been omitted for clarity.



535

Figure 2. Established formation routes to form IEPOX and INHE via the OH oxidation of stable hydroperoxide intermediates. Additional isomers and reaction pathways have been omitted for clarity.



540

Figure 3. The alkoxy-epoxidation pathway to form a range of nitrated epoxides, as proposed by Vereecken et al. 2021. Additional isomers and reaction pathways have been omitted for clarity.

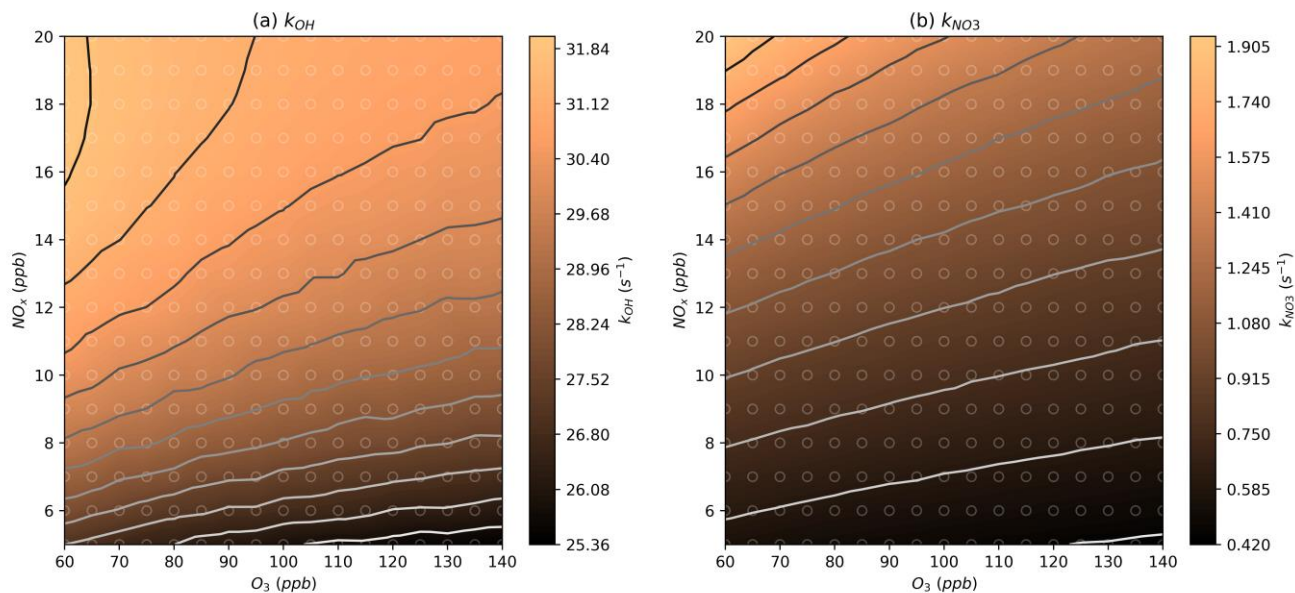
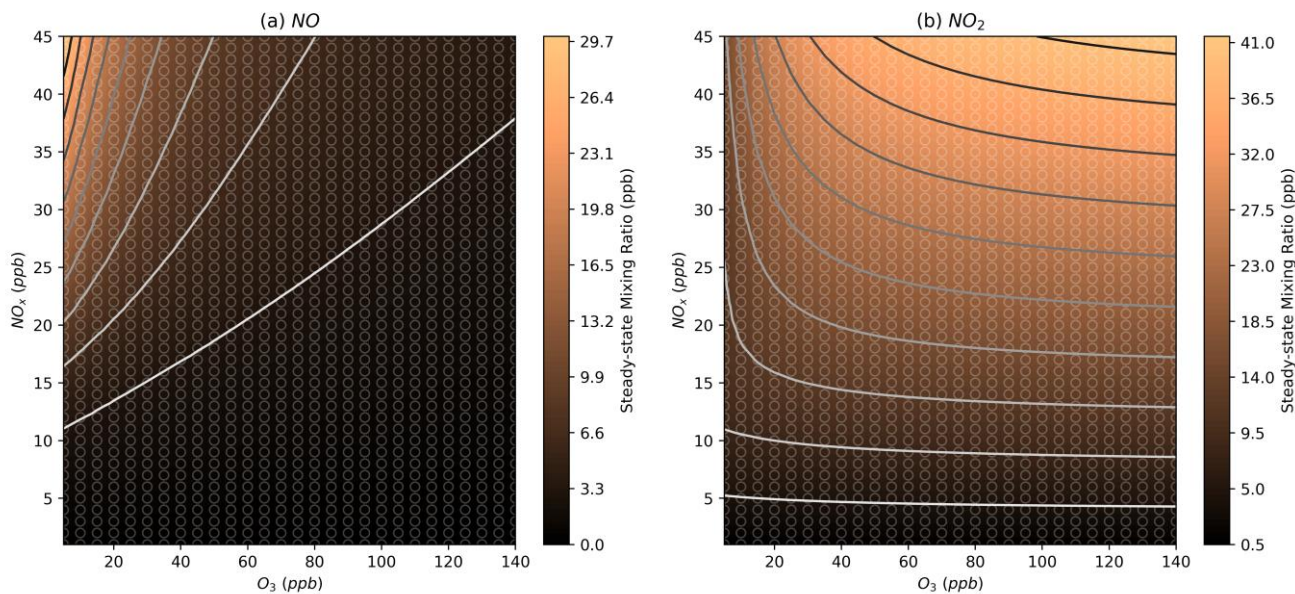


Figure 4. Modelled steady-state k_{OH} and k_{NO_3} values at different NO_x and O_3 mixing ratios. Further details on interpreting these plots is given in Section 2.2.



545 Figure 5. Modelled steady-state mixing ratios of NO and NO_2 at different NO_x and O_3 mixing ratios. Further details on interpreting these plots is given in Section 2.2.

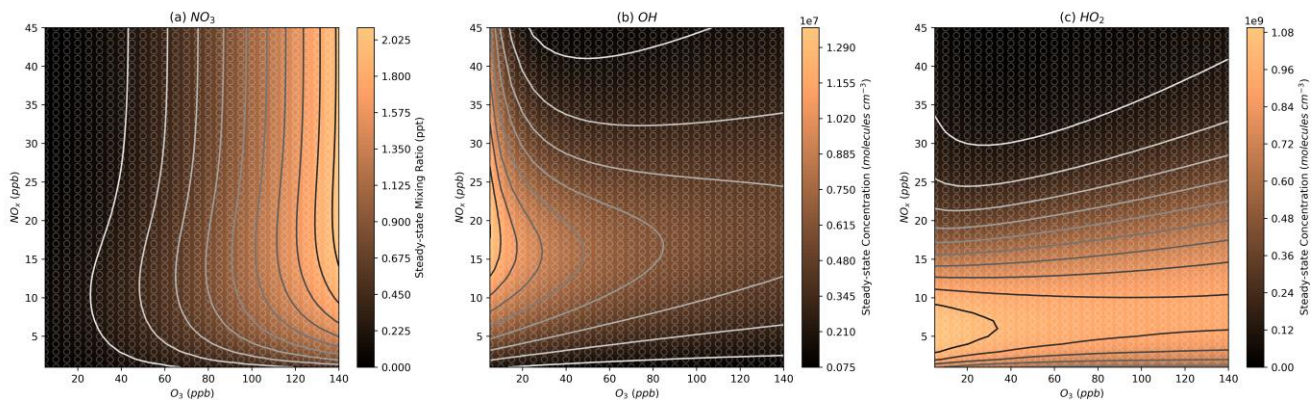


Figure 6. Modelled steady-state concentrations of NO_3 , OH , and HO_2 at different NO_x and O_3 mixing ratios. Further details on interpreting these plots is given in Section 2.2.

550

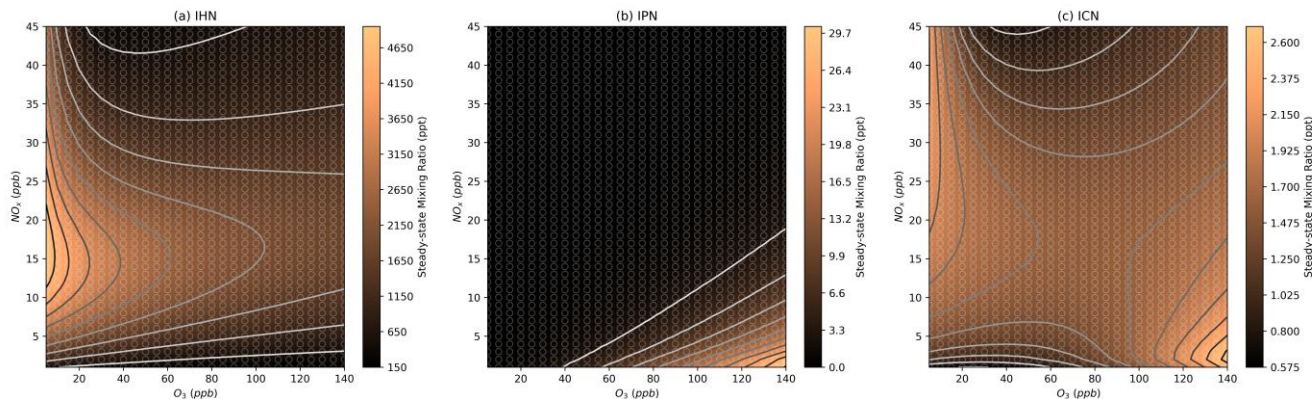
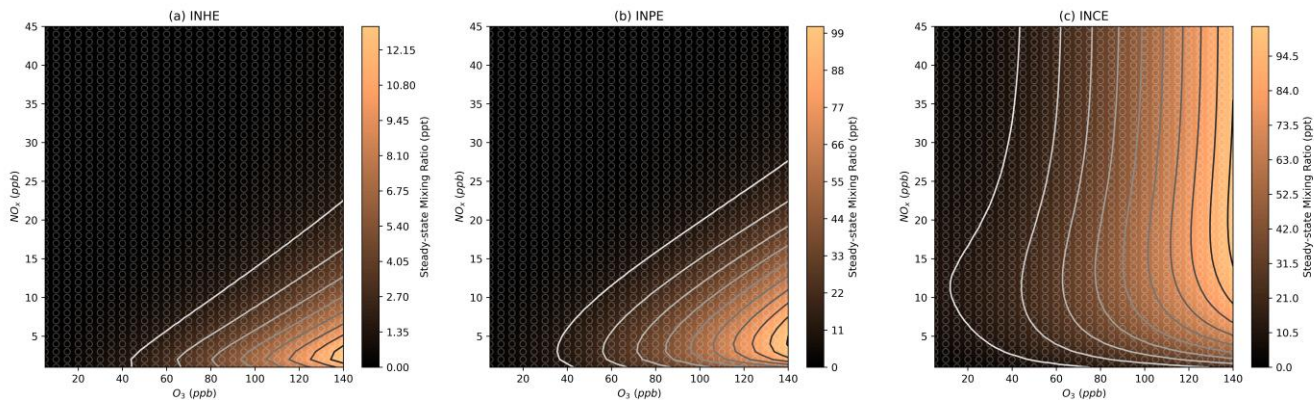
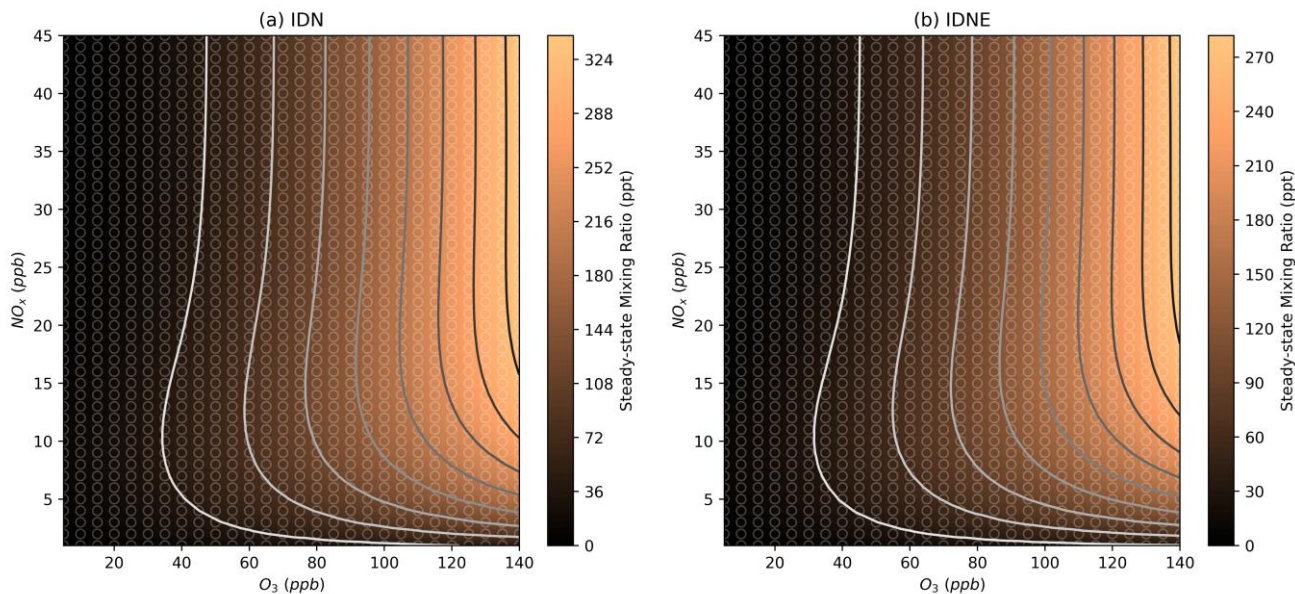


Figure 7. Modelled steady-state concentrations of isoprene hydroxynitrate (IHN), isoprene carbonylnitrate (ICN), and isoprene hydroperoxynitrate (IPN) at different NO_x and O_3 mixing ratios. Further details on interpreting these plots is given in Section 2.2.



555 **Figure 8.** Modelled steady-state concentrations of isoprene hydroxynitrooxyepoxide (INHE), isoprene carbonylnitrooxyepoxide (INCE), and isoprene hydroperoxynitrooxyepoxide (INPE) at different NO_x and O_3 mixing ratios. Further details on interpreting these plots is given in Section 2.2.



560 **Figure 9.** Modelled steady-state concentrations of isoprene dinitrate (IDN) and isoprene dinitrooxyepoxide (IDNE) at different NO_x and O_3 mixing ratios. Further details on interpreting these plots is given in Section 2.2.

Isoprene = 1 ppb $O_3 = 50$ ppb

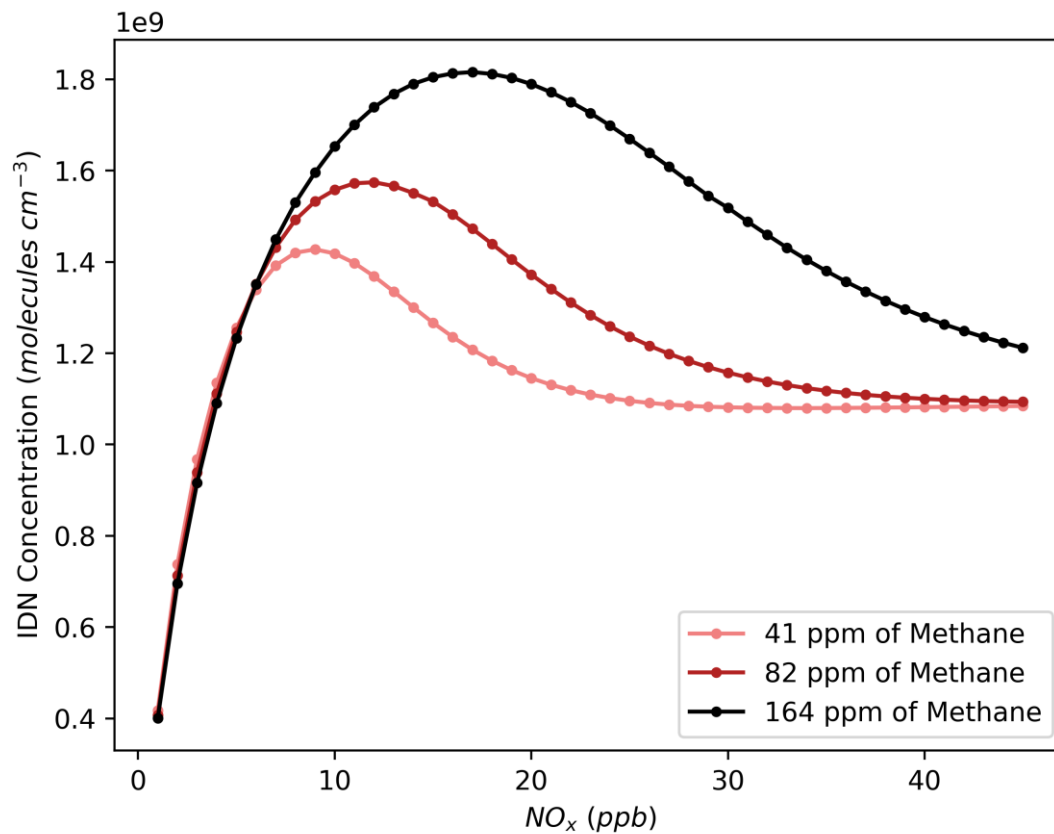
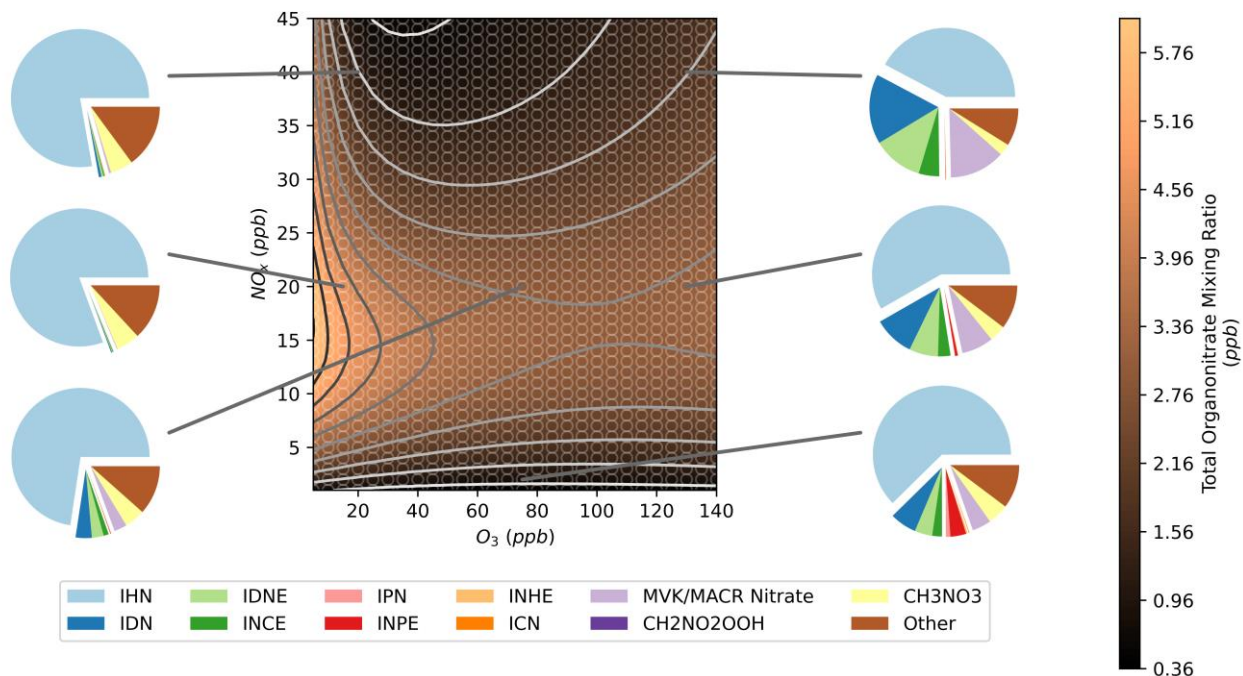
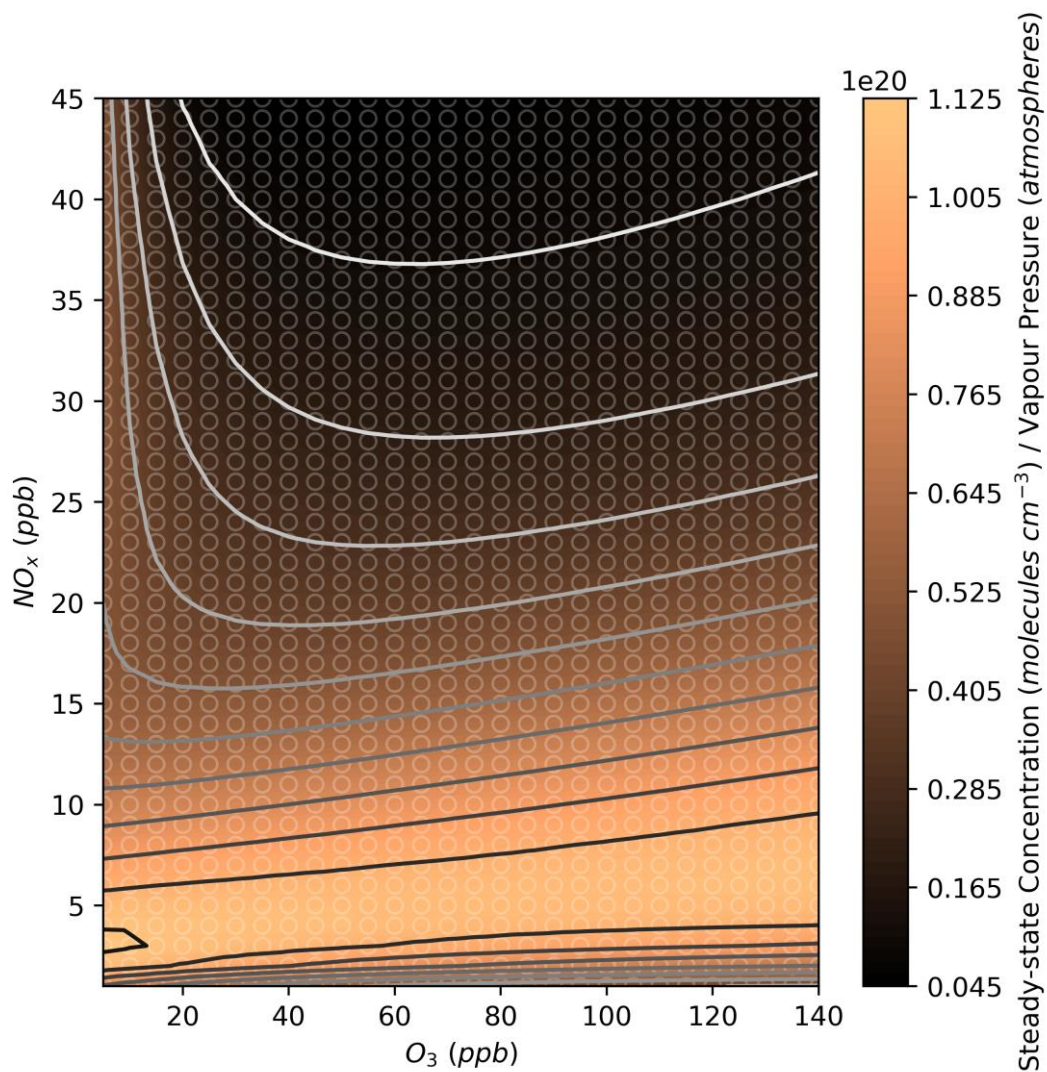


Figure 10. Modelled steady-state concentrations of IDN with changing NO_x in models runs with 50 ppb of O₃ and different mixing ratios of NO_x and additional methane.



565 **Figure 11. Modelled steady-state concentrations of the total organonitrates at different NO_x and O_3 mixing ratios along with the composition of the total organonitrates at selected NO_x and O_3 mixing ratios. Further details on interpreting these plots is given in Section 2.2.**



570 **Figure 12.** Modelled steady-state concentrations of the total organonitrates normalised to each compound's estimated vapour pressure at different NO_x and O_3 mixing ratios. Further details on interpreting these plots is given in Section 2.2.

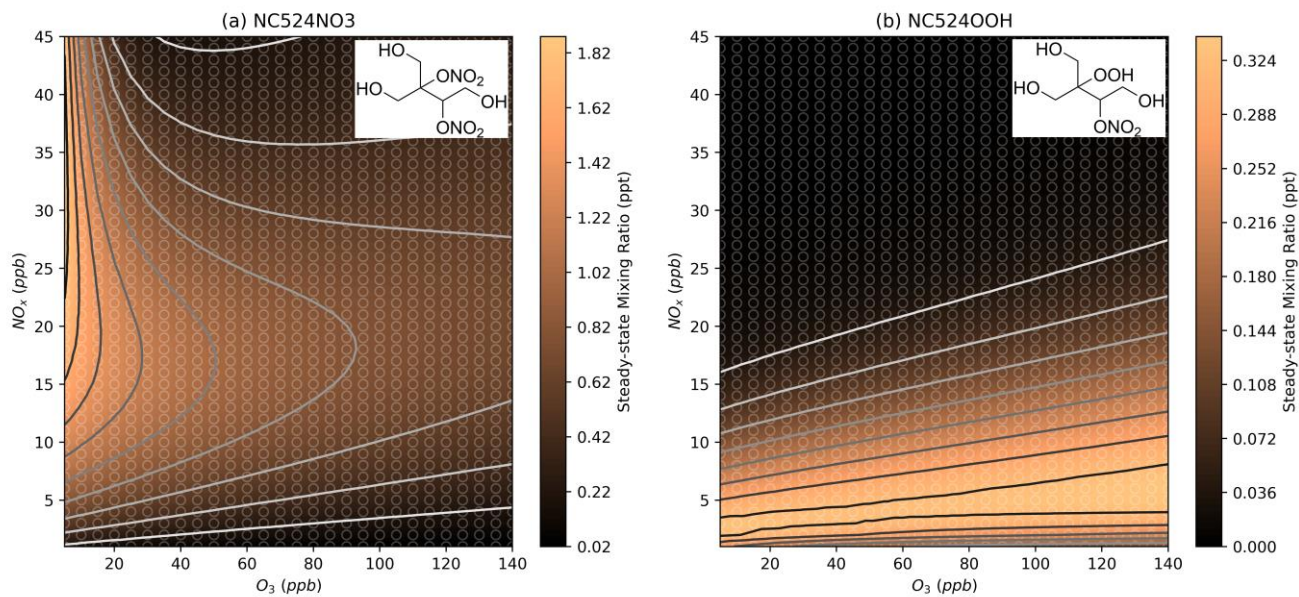
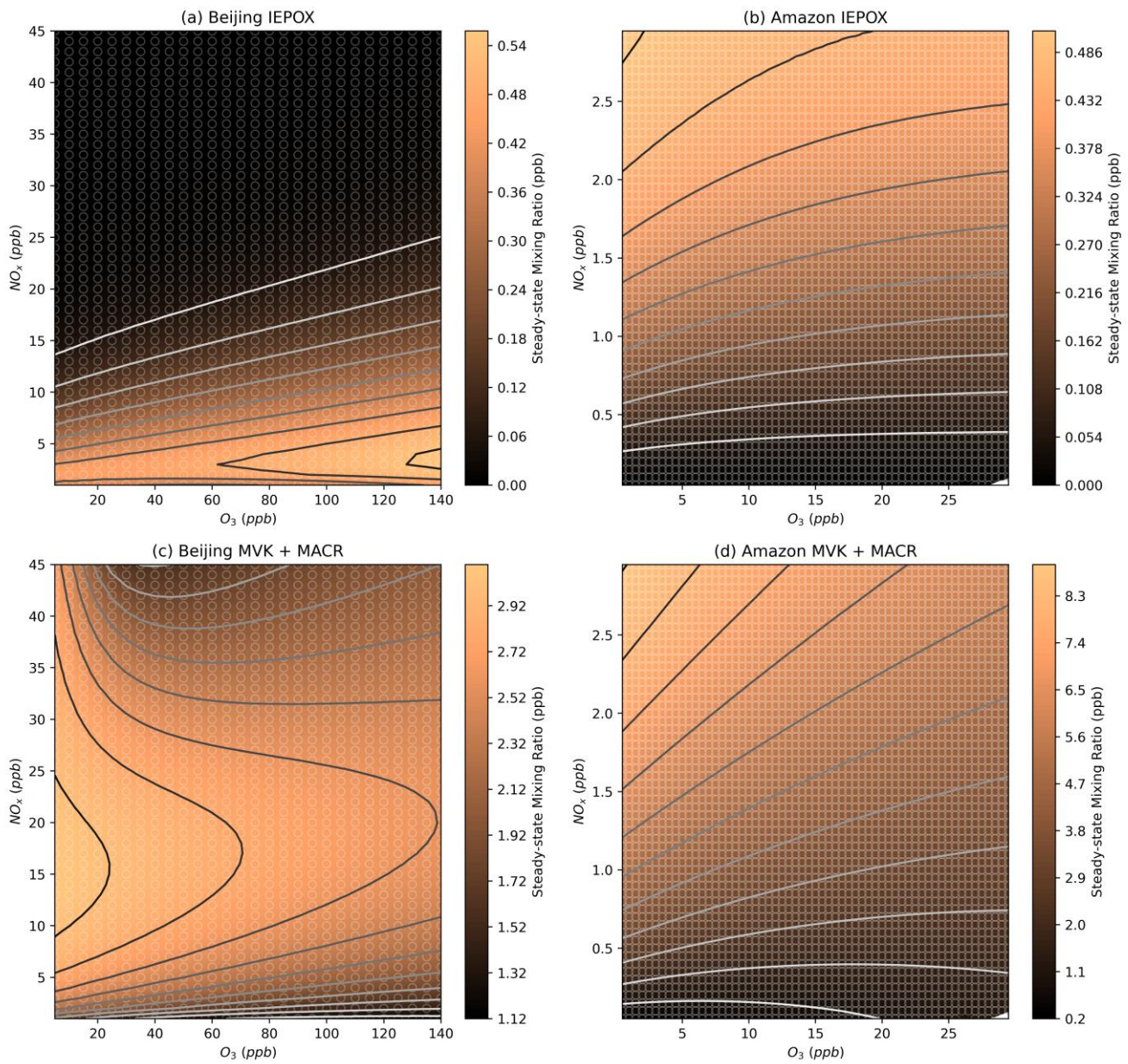


Figure 13. Modelled steady-state concentrations of the MCM species NC524NO3 and NC524OOH at different NO_x and O_3 mixing ratios. Further details on interpreting these plots is given in Section 2.2.



575 **Figure 14.** Modelled steady state IEPOX and MVK + MACR concentrations for the Beijing (a,c) and Amazon (b,d) models.